



FULL PAPER

Efficient aerial oxidation of different types of alcohols using ZnO nanoparticle–MnCO₃–graphene oxide composites

Syed Farooq Adil¹ | Mohamed E. Assal¹ | Mohammed Rafi Shaik¹ |
Mufsir Kuniyil¹ | Azhar Hashmi² | Mujeeb Khan¹ | Aslam Khan³ |
Muhammad Nawaz Tahir⁴ | Abdulrahman Al-Warthan¹ |
Mohammed Rafiq H. Siddiqui¹

¹Chemistry Department, College of Science, King Saud University, P.O. 2455, Riyadh, 11451, Kingdom of Saudi Arabia

²SABIC Technology and Innovation, Riyadh, Kingdom of Saudi Arabia

³King Abdullah Institute for Nanotechnology, King Saud University, Riyadh, 11451, Kingdom of Saudi Arabia

⁴Chemistry Department, King Fahd University of Petroleum and Materials, Dhahran, 31261, Kingdom of Saudi Arabia

Correspondence

Syed Farooq Adil and Mohammed Rafiq H Siddiqui, Chemistry Department, College of Science, King Saud University, P.O. 2455, Riyadh 11451, Kingdom of Saudi Arabia.
Email: sfadil@ksu.edu.sa; rafiqs@ksu.edu.sa

Funding information

Deanship of Scientific Research, King Saud University, Grant/Award Number: RG-1436-032

Graphene–metal nanocomposites have been found to remarkably enhance the catalytic performance of metal nanoparticle-based catalysts. In continuation of our previous report, in which highly reduced graphene oxide (HRG)-based nanocomposites were synthesized and evaluated, we present nanocomposites of graphene oxide (GRO) and ZnO nanoparticle-doped MnCO₃ ([ZnO–MnCO₃/(1%)GRO]) synthesized via a facile, straightforward co-precipitation technique. Interestingly, it was noticed that the incorporation of GRO in the catalytic system could noticeably improve the catalytic efficiency compared to a catalyst (ZnO–MnCO₃) without GRO, for aerial oxidation of benzyl alcohol (BzOH) employing O₂ as a nature-friendly oxidant under base-free conditions. The impacts of various reaction factors were thoroughly explored to optimize reaction conditions using oxidation of BzOH to benzaldehyde (BzH) as a model substrate. The catalysts were characterized using X-ray diffraction, thermogravimetric analysis, Fourier transform infrared spectroscopy, field-emission scanning electron microscopy, Energy dispersive X-ray spectroscopy (EDX), Brunauer–Emmett–Teller (BET), and Raman spectroscopy. The (1%) ZnO–MnCO₃/(1%)GRO exhibited significant specific activity (67 mmol.g⁻¹.hr⁻¹) with full conversion of BzOH and >99% BzH selectivity within just 6 min. The catalytic efficiency of the (1%)ZnO–MnCO₃/(1%)GRO nanocomposite was significantly better than the (1%)ZnO–MnCO₃/(1%)HRG and (1%)ZnO–MnCO₃ catalysts, presumably due to the existence of oxygen-possessing groups on the GRO surface and as well as a very high surface area that could have been instrumental in uniformly dispersing the active sites of the catalyst, i.e., ZnO–MnCO₃. Under optimum circumstances, various kinds of alcohols were selectively transformed to respective carbonyls with full convertibility over the (1%)ZnO–MnCO₃/(1%)GRO catalyst. Furthermore, the highly effective (1%)ZnO–MnCO₃/(1%)GRO catalyst could be successfully

reused and recycled over five consecutive runs with a marginal reduction in its performance and selectivity.

KEYWORDS

graphene, MnCO₃, nanocomposite, oxidation, ZnO nanoparticles

1 | INTRODUCTION

Transforming alcohols by catalytic oxidation to their corresponding aldehydes and ketones plays a fundamental role in various industries, including the agro-chemical, fragrance, dyestuff, insecticide, cosmetics, flame-retardant, flavor, vitamin, and drug industries.^[1] It has been reported that this oxidation alone participated in around 25% of global organic chemical production and the worldwide market for this reaction has been evaluated to be approximately US\$50 billion.^[2] Traditionally, the oxidation of alcohols has relied on the use of costly and undesirable stoichiometric oxidants such as dichromate, hypochlorite, and permanganate etc., which produce large amount of hazardous by-products.^[3] Environmental and economic concerns have led scientists to replace undesirable conventional stoichiometric methods with the clean catalytic oxidation protocols utilizing molecular O₂ or air as benign oxidizing agents in order to minimize the environmentally unacceptable wastes.^[4] Recently, many results have been reported employing noble metal-based catalysts such as Au, Pd, Ru, etc.^[5] Nevertheless, these precious metals suffer from many drawbacks owing to their rarity, toxicity, and high cost.^[6] Therefore, it is highly desirable to find cheaper replacements for expensive metal and waste-generating catalysts. In this regard, non-noble transitional metals (e.g., Fe, Co, Mo, Cu, Cr, and Zr) have been widely explored.^[7] In the past two decades, it has been found that mixed metal oxide-based catalysts have higher catalytic performance and stability than their monometallic counterparts, which has been ascribed to geometric and electronic effects as well as the massive increase in surface area and more active exposed faces.^[8] Notwithstanding, small nanoparticles (NPs) suffer from instability and are easily aggregated due to their huge surface energy, which reduces their reactivity.^[9] In order to resolve this dilemma, researchers found that immobilizing active species utilizing various supports.^[10]

Among the various types of metal oxides, manganese oxides (MnO_x) have attracted enormous interest because of their novel and extraordinary characteristics, including their high activity, low cost, nontoxic nature, and many morphologies and structures, and they have been widely used in numerous fields such as sensors, supercapacitors, fuel cells, batteries and catalysis.^[11] Importantly,

manganese-based catalysts are widely employed as effective oxidative catalysts for catalytic alcohol oxidation to their corresponding carbonyls and have afforded outstanding efficiency and selectivity.^[12]

Graphene is a two-dimensional (2D) one-atom sheet of sp² carbon atoms that are tightly packed in a honeycomb crystal structure with a huge theoretical surface area of 2630 m²/g. Graphene-based nano-sized materials have gained much attention owing to the enhancement of their intrinsic electronic, thermal, optical, mechanical and catalytic properties due to the inclusion of graphene in the system.^[13] Because of these novel and exceptional characteristics, graphene and its derivatives, particularly graphene oxide (GRO) and highly reduced graphene oxide (HRG), have been extensively employed for the catalytic conversion of organic compounds in reactions such as reduction, oxidation, Suzuki coupling, Heck coupling, and so on.^[14] GRO and HRG are widely used as exemplary catalyst supports for catalytically active metal NPs due to their amazing properties, such as outstanding chemical stability, extremely high surface area, and facile recyclability of metals from reused catalysts.^[15] In particular, GRO is considered to be an excellent catalyst support due to its superior layered structure and surface properties. The GRO plane possesses myriad oxygen-carrying functionalities, which provide its moderate acidic and oxidizing properties.^[16] Additionally, these oxygenic possessing groups can also act as anchoring sites to immobilize metallic or metallic oxide NPs on the GRO plane, therefore producing numerous opportunities to form new types of catalysts.^[17] Different metal or metal oxide NPs, such as Pd,^[18] Ag,^[19] MnO₂,^[11] and Fe₂O₃,^[20] have been deposited on GRO flakes and afford excellent performance and selectivity. In particular, GRO-based metal NP composites have been used as efficacious catalysts for the oxidation of numerous organic compounds, for example alcohols,^[11] alkenes,^[21] amines,^[22] alkyl benzene,^[23] and benzene.^[24]

In our previous studies, we reported a variety of graphene-based nanocomposites and it was found that the catalytic properties improve considerably. In continuation of this work,^[9,25] the present study was designed to understand the effect of the inclusion of graphene oxide in (1%)ZnO-MnCO₃, which was found to possess substantial oxidation properties. This study involves a comparative catalytic estimation between undoped catalyst

i.e. ((1%)ZnO-MnCO₃ without graphene oxide) and ZnO-MnCO₃ with GRO doping for liquid-phase oxidation of various kinds of alcohols (Scheme 1). Undoped catalyst i.e. (1%)ZnO-MnCO₃ and (1%)ZnO-MnCO₃/(1%)GRO nanocomposites were synthesized by a facile and straightforward co-precipitation technique and their catalytic properties were estimated. Notably, this is the first report on the ZnO doped MnCO₃/GRO nanocomposite as an oxidation catalyst for aerial alcohol oxidation and the catalytic activity of ZnO-MnCO₃ catalyst was evaluated after doping it with GRO. Furthermore, the as-fabricated materials were characterized by X-ray diffraction (XRD), thermogravimetric analysis (TGA), Fourier transform infrared spectroscopy (FT-IR), field-emission scanning electron microscopy (FE-SEM), Energy dispersive X-ray spectroscopy (EDX), Brunauer-Emmett-Teller (BET), and Raman spectroscopy.

2 | EXPERIMENTAL

2.1 | Synthesis of GRO and HRG

First, GRO was prepared from pure graphite via Hummers' technique.^[26] Subsequently, GRO was reduced using hydrazine hydrate to HRG. The full procedure is given in the Supporting Information.

2.2 | Synthesis of (1%)ZnO-MnCO₃/(X%) GRO nanocomposite

First, we synthesized ZnO-doped MnCO₃ via a co-precipitation procedure by mixing stoichiometric amounts of Mn(NO₃)₂ and Zn(NO₃)₂ dissolved in distilled water in a round-bottomed flask at 100°C with strong stirring. A solution of NaHCO₃ (0.5 M) was added dropwise until the pH of the solution reached 9. The stirring was

continued for 3 hr at 100°C, later it was continued overnight at room temperature (RT). The reaction mixture was filtered using centrifugation and dried at 70°C overnight. The obtained material was heated in a furnace at 300°C. The synthesized GRO was dried at 70°C, milled in a milling machine, and mixed with ZnO-doped MnCO₃ proportionately to yield (1%) ZnO-MnCO₃/(X%) GRO nanocomposite.

2.3 | Catalyst characterization

The obtained materials were characterized by various instruments and all experimental details are given in the Supporting Information.

2.4 | Catalytic study

The general method for aerial oxidation of alcohols is described in the Supporting Information.

2.5 | Reusability tests

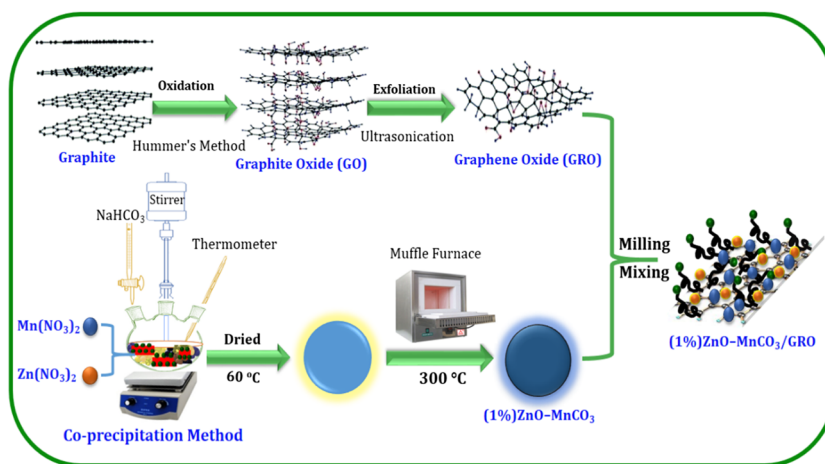
After the end of the first oxidation reaction, the used catalyst was separated by a simple centrifuge process, then washed several times with toluene and dried at 100°C for 4 hrs for next use. The dried catalyst was employed for the next run under optimal conditions.

3 | RESULTS AND DISCUSSION

3.1 | Characterizations

XRD was used to study the crystal structures of the prepared samples. Figure 1 shows the XRD patterns of the

SCHEME 1 Schematic presentation of the fabrication of (1%)ZnO-MnCO₃/(1%)GRO nanocomposite



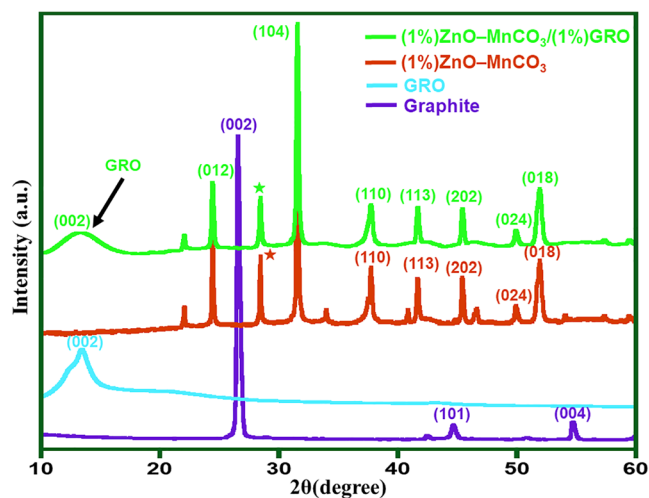


FIGURE 1 XRD patterns of graphite, GRO, undoped (1%) ZnO-MnCO₃ catalyst, and (1%) ZnO-MnCO₃/(1%) GRO nanocomposite

pristine graphite, GRO, (1%) ZnO-MnCO₃, and (1%) ZnO-MnCO₃/(1%) GRO. The obtained XRD results are displayed in Figure 1. The sharp diffraction peak of graphite situated at $2\theta = 26.5^\circ$ corresponds to the (002) plane with an interlayer d-spacing of 3.4 Å.^[27] The appearance of the GRO characteristic band at $2\theta = 11.62^\circ$ corresponds to the (002) crystal plane, and the disappearance of graphite characteristic peak at $2\theta = 26.5^\circ$, confirms that efficient oxidation of graphite to GRO nanosheets and presence of oxygen-carrying functionalities on the GRO's surfaces.^[28] The shift in 2θ is due to an increase in the interplanar distance from 3.4 to 6.4 Å for graphite and GRO, which might be ascribed to the inclusion of myriad oxygen-containing groups on the surface of the GRO nanosheets.^[29] The XRD pattern of the undoped catalyst (without GRO), that is, (1%) ZnO-MnCO₃, is very much in accordance with the reported data for rhodochrosite MnCO₃ (JCPDS No. 1-0981), however, the reflections labelled with asterisks could be due to the presence of ZnO.^[30] As regards the (1%) ZnO-MnCO₃/(1%) GRO pattern, the GRO characteristic peak at 11.8° was seen in addition to the diffraction signals of rhodochrosite MnCO₃, indicating the presence of GRO in the as-fabricated nanocomposite.

The FT-IR spectra of GRO and (1%) ZnO-MnCO₃/(1%) GRO are depicted in Figure 2. The FT-IR spectrum of GRO shows a wide-ranging peak around 3430 cm⁻¹, originating from the presence of the stretching vibration of hydroxyl groups or physisorbed H₂O present on the GRO surface. The absorption peak at 1740 cm⁻¹ corresponds to (C=O) stretching of carboxylic groups and the peak at ~1630 cm⁻¹ corresponds to the stretching vibration of the carbon skeleton (C-C/C=C) from unoxidized graphitic

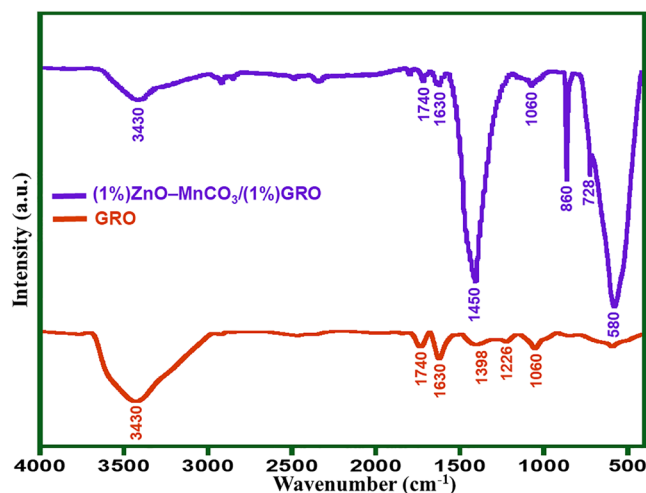


FIGURE 2 FT-IR spectra of GRO and (1%) ZnO-MnCO₃/(1%) GRO nanocomposite

areas.^[31] The three peaks at 1398, 1226, and 1060 cm⁻¹ can be ascribed to the stretching of (C-OH), (C-O-C), and (C-O) groups, respectively.^[32] Unsurprisingly, the spectrum for (1%) ZnO-MnCO₃/(1%) GRO displayed the characteristic peaks of most of the oxygenic groups i.e. 1738 cm⁻¹ (C=O) and 1060 cm⁻¹ (C-O). In addition, there were two intense peaks at 860 and 728 cm⁻¹, and a wide-ranging peak at approximately 1450 cm⁻¹, which are fingerprint peaks for manganese carbonate.^[33] In addition, the intensive strong peak at 580 cm⁻¹ corresponds to vibrations of various manganese oxides.^[34]

Raman spectroscopy is enormously informative characterization instrument for the structural identification of graphene-based materials. Figure 3 shows the Raman analysis of (1%) ZnO-MnCO₃ and (1%) ZnO-MnCO₃/(1%)

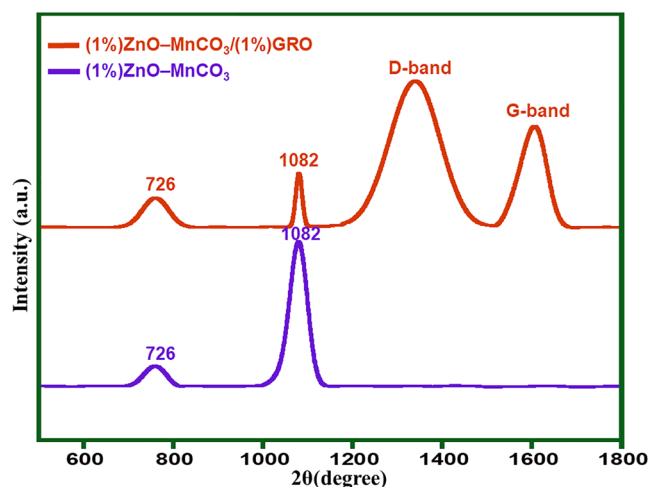


FIGURE 3 Raman spectra of (1%) ZnO-MnCO₃ catalyst (without GRO) and (1%) ZnO-MnCO₃/(1%) GRO nanocomposite

GRO. As expected, the Raman patterns of (1%)ZnO–MnCO₃ and (1%)ZnO–MnCO₃/(1%)GRO nanocomposite showed two fingerprint bands of MnCO₃ situated at approximately 726 and 1082 cm⁻¹, proving the presence of MnCO₃ in both (1%)ZnO–MnCO₃ and (1%)ZnO–MnCO₃/(1%)GRO nanocomposite.^[35] In addition, the presence of GRO in the (1%)ZnO–MnCO₃/(1%)GRO was confirmed by the appearance of two characteristic peaks at ~1592 and 1348 cm⁻¹, usually denoted as the D-band and G-band, respectively.^[36] The D-band is commonly associated with defects or disorder in the graphite structure and the G-band is associated with the vibrations of sp² carbon atoms of a well-ordered structure.^[37] Compared with GRO, the G-band in the (1%)ZnO–MnCO₃/(1%)GRO nanocomposite was shifted by 9 cm⁻¹ from 1584 to 1593 cm⁻¹, whilst a slight shift was noticed in the D-band from 1344 to 1348 cm⁻¹, confirming the intensive coupling between the MnCO₃ and GRO.^[14c] Furthermore, we did not observe a 2D peak in our spectra. The 2D peak is a secondary D peak, which is the largest intensity peak in single-layer graphene, but broadens (into four peaks) and reduces in intensity in multilayer graphene. Normally, there is not much difference as you can observe from graphite if it is more than five layers.

This scenario, in principle, can be caused by the splitting of phonon bands or electron bands. This could be attributed to the splitting of electron bands because the splitting of phonon branches, from a single layer to a bilayer, is calculated to be less than 1.5 cm⁻¹ which is very small compared with the experimentally observed 2D splitting.

The morphology of the as-fabricated (1%)ZnO–MnCO₃ and (1%)ZnO–MnCO₃/(1%)GRO nanocomposite produced via an *ex situ* hybridization method was studied using high-resolution FE-SEM (Figure 4a–d). The FE-SEM micrographs for the (1%)ZnO–MnCO₃ catalyst displayed well-defined cuboidal morphology particles of micro size, but the micrographs for the (1%)ZnO–MnCO₃/(1%)GRO nanocomposite interestingly showed the presence of graphene sheets on the surface alongside the (1%)ZnO–MnCO₃ (Figure 4d). High-resolution FE-SEM elemental mapping was also carried out for (1%)ZnO–MnCO₃/(1%)GRO nanocomposite, as shown in Figure 5. The mapping micrographs display the mapped elements in four colors: turquoise (oxygen), red (manganese), yellow (zinc), and purple (carbon). It is clear that the zinc oxide is highly dispersed on the surface of MnCO₃, which could explain the increase in the specific surface area. However, elemental mapping of oxygen and carbon revealed their presences in

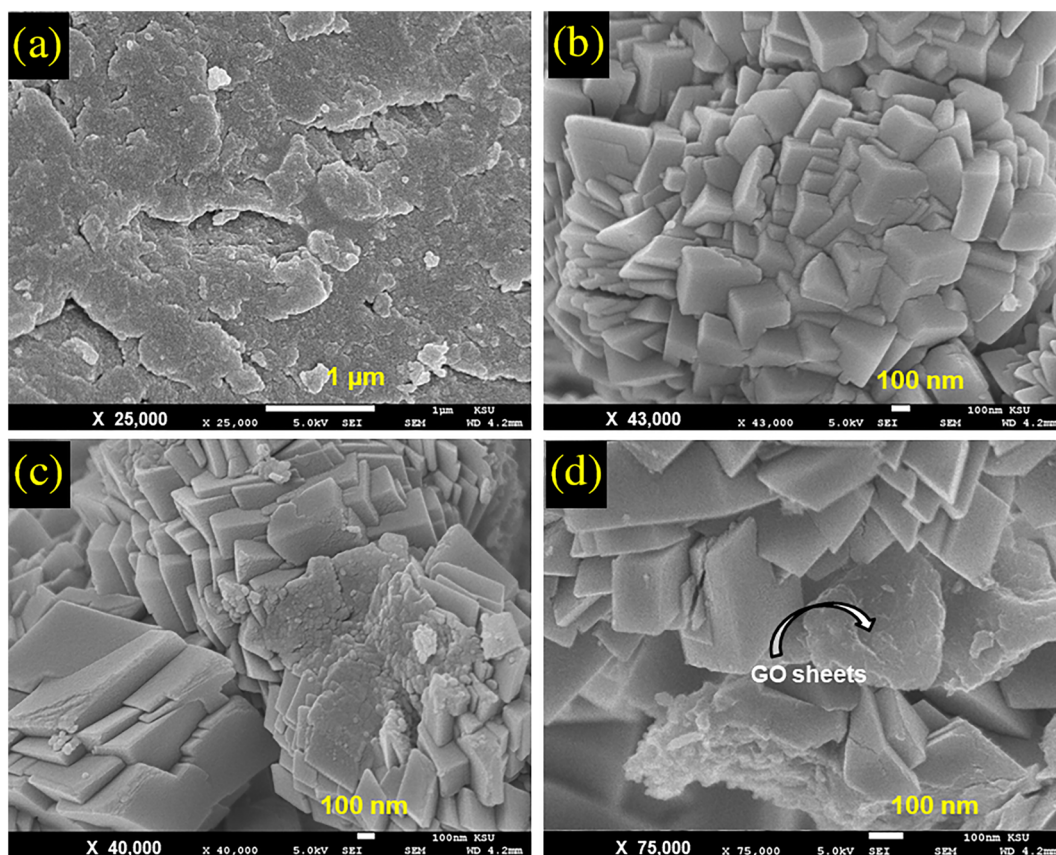


FIGURE 4 FE-SEM images of (a) GRO, (b) (1%)ZnO–MnCO₃, (c) (1%)ZnO–MnCO₃/(1%)GRO, and (d) (1%)ZnO–MnCO₃/(1%)GRO showing graphene oxide sheets as thin layers in the nanocomposite

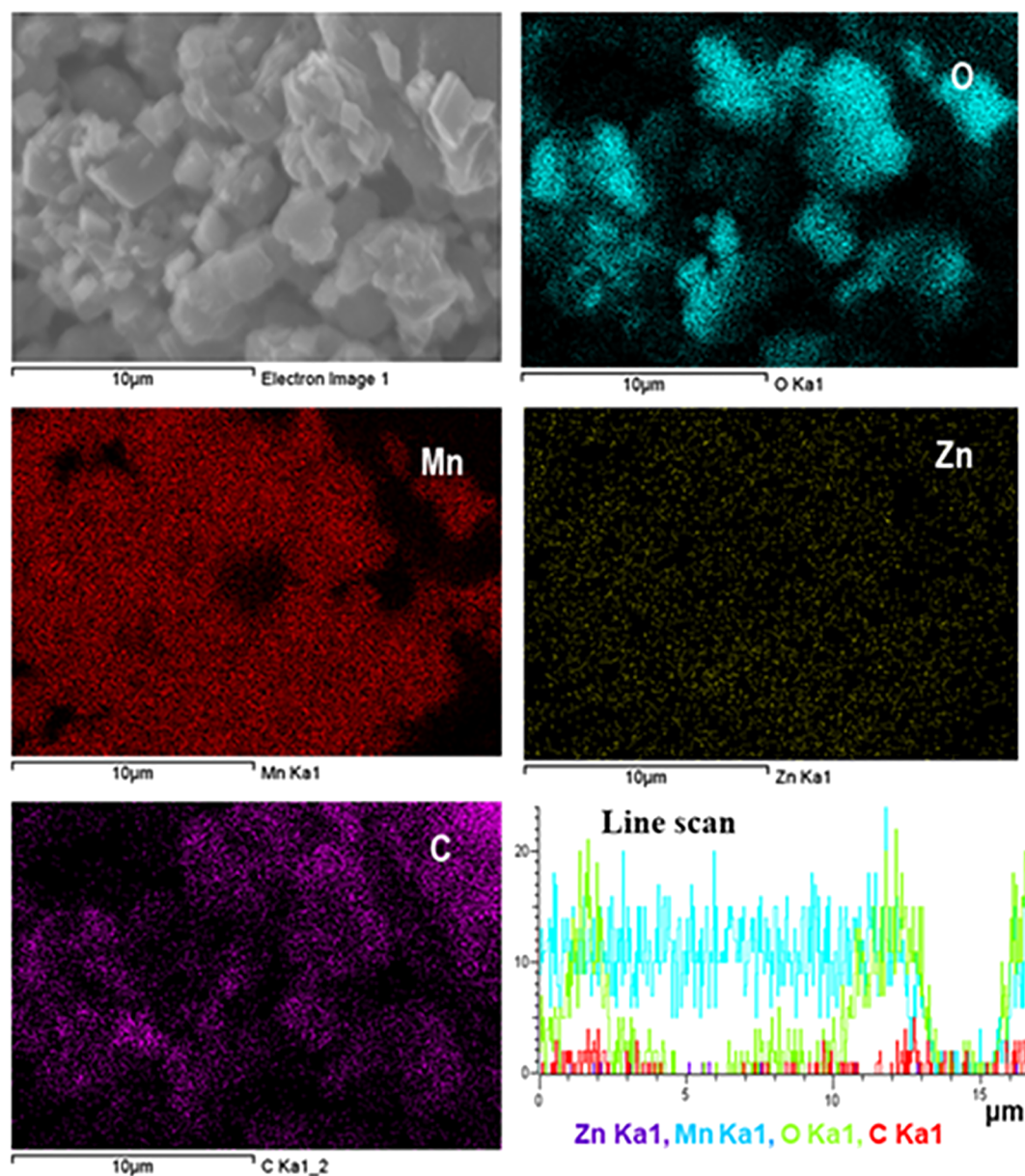


FIGURE 5 Elemental mapping and line scan profile of (1%)ZnO–MnCO₃/(1%)GRO

the entire scan area, which can be attributed to the CO₃ species of MnCO₃ and the graphene oxide in the catalytic system. Furthermore, the line scan mapping diagram (Figure 5) and the EDX spectrum (Supporting Information Figure S1) confirmed the existence of Zn and C in the MnCO₃ samples with homogeneity and the existence of Zn, Mn, O, and C, respectively.

Thermal stability was examined using TGA in order to determine the thermal property of (1%)ZnO–MnCO₃/(1%)GRO nanocomposite and compare it with the thermal degradation properties of the graphite, GRO, and undoped catalyst (1%)ZnO–MnCO₃ precursors, as described in Figure 6. Samples were heated from RT to 800°C at a heating rate of 10°C/min in a nitrogen atmosphere. It can

be seen that the thermal degradation property of graphene oxide is much lower than that of graphite because of the presence of oxygenic possessing groups on the surface of the GRO. The TGA graph of graphite shows an entire weight loss of ~1%.^[38] GRO is thermally unstable and even at 100°C it begins to eliminate physisorbed water and moisture followed by a fundamental weight loss of 43% at 200–370°C owing to the pyrolysis of the oxygenated functionalities.^[39] Eventually, GRO loses about 11% of its weight, presumably due to the thermal decomposition of the carbon skeleton from 370 to 800°C.^[40] These thermal results are in good accordance with previously reported work.^[41] The (1%)ZnO–MnCO₃/(1%)GRO loses ~25% of its total weight at 800°C, which is higher than the weight loss

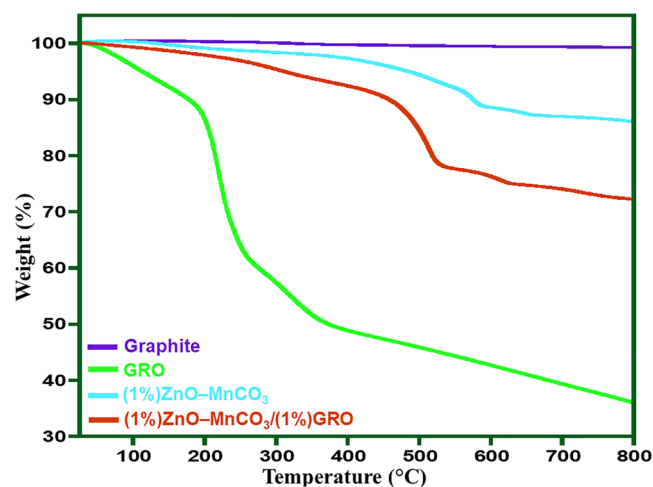
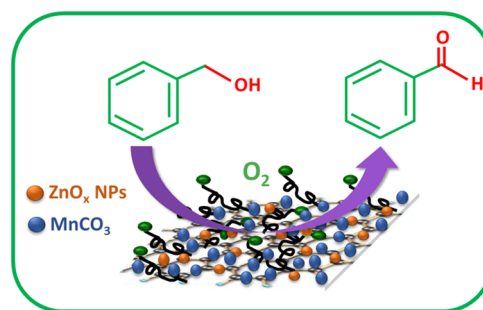


FIGURE 6 TGA thermograms of graphite, GRO, (1%)ZnO-MnCO₃, and (1%)ZnO-MnCO₃/(1%)GRO

obtained from the degradation curve of undoped (1%) ZnO-MnCO₃ catalyst, indicating enhancement of the thermal stability of the catalyst.

To determine the specific surface areas of the obtained catalysts and assess their relation with the efficacy of the catalytic protocol for benzyl alcohol (BzOH) oxidation, BET analysis was used. Table 1 shows that the specific surface area of the undoped catalyst, that is, without graphene doping, (1%)ZnO-MnCO₃, is approximately 120 m²/g. As anticipated, the surface areas of the nanocomposites after doping the catalyst with GRO and HRG were considerably increased to 245 and 239 m²/g, respectively. It is important to mention that the catalytic data are in accordance with the surface area BET measurements. Fortunately, the catalytic effectiveness after incorporating GRO and HRG in the catalyst, that is, (1%)ZnO-MnCO₃/(1%)GRO and (1%)ZnO-MnCO₃/(1%)HRG, also markedly increased. Hence, it can be stated that the inclusion graphene (GRO or HRG) has a positive impact on the surface area of the as-fabricated catalysts, which in turn enhances the catalytic activity of the as-obtained nanocomposites.



SCHEME 2 Schematic depiction of BzOH oxidation utilizing O₂ over the prepared nanocomposite

3.2 | Catalytic application

The main aim of this work was to oxidize various kinds of alcohols to the corresponding carbonyls with superior yields after short times using molecular O₂ as an environmentally friendly oxidant without the addition of any surfactants or bases under mild conditions. To realize this objective, we used GRO as a co-dopant for the ZnO-MnCO₃ catalyst in the aerial oxidation of BzOH as a compound model under base-free conditions, as described in Scheme 2. The reaction conditions were systematically optimized in detail as shown in Figures 7–10 and Tables 1 and 2.

3.2.1 | Influence of wt% of GRO

Generally, the catalytic efficacy of the catalyst for alcohol oxidation is significantly enhanced after using graphene or its derivatives as a supporting material.^[7a,19,42] In our previously reported work, we concluded that ZnO NPs were found to be exemplary promoters for MnCO₃ and (1%)ZnO-MnCO₃ catalyst annealed at 300°C exhibited outstanding catalytic activity for selective alcohol oxidation.^[30] Hence, for the current study, the (1%)ZnO-MnCO₃ catalyst was selected with a focus to further

TABLE 1 The catalytic efficiencies of various catalysts

Entry	Catalyst	Conversion (%)	Specific activity (mmol.g ⁻¹ .hr ⁻¹)	Selectivity (%)
1	GRO	2.4	1.6	<99
2	(1%)ZnO-MnCO ₃	69.1	46.1	<99
3	(1%)ZnO-MnCO ₃ /(1%)GRO	100.0	66.7	<99
4	(1%)ZnO-MnCO ₃ /(3%)GRO	92.3	61.6	<99
5	(1%)ZnO-MnCO ₃ /(5%)GRO	79.2	52.8	<99
6	(1%)ZnO-MnCO ₃ /(7%)GRO	72.6	48.4	<99

Note. Conditions: 2 mmol BzOH, 10 ml toluene, 300 mg catalyst, O₂ 20 ml/min, 100°C, 6 min.

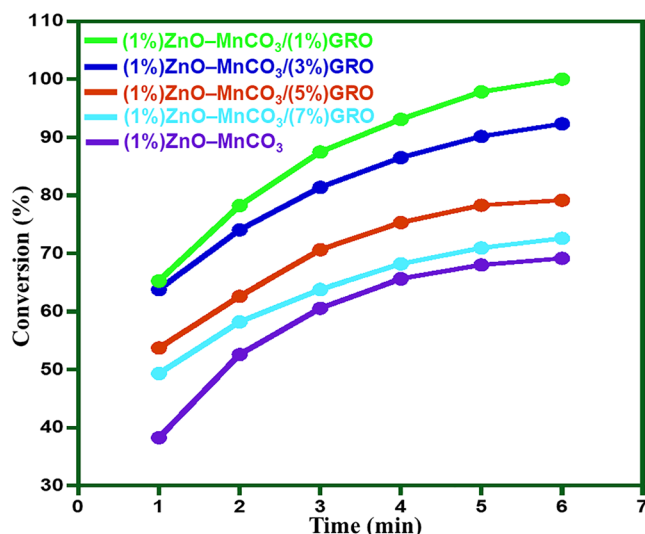


FIGURE 7 Graphical representation of BzOH oxidation over catalysts with various percentages of GRO

improve it by incorporating GRO in it to increase its catalytic activity.

Initially, we assessed the efficacy of only GRO for the aerial oxidation of BzOH using O₂ as an eco-friendly oxidant at 100°C. It was noticed that GRO alone (without ZnO-MnCO₃) did not produce any oxidative product with BzOH (1, entry 1). The catalytic activities of various (1%) ZnO-MnCO₃/(X%)GRO nanocomposites (where X = 0–7) in which the percentage of GRO was changed from 1 to 7 (wt/wt%) and its efficiency was investigated for oxidation of BzOH. The results are shown in Table 1 and Figure 7. They reveal that the catalyst without GRO, i.e. (1%)ZnO-

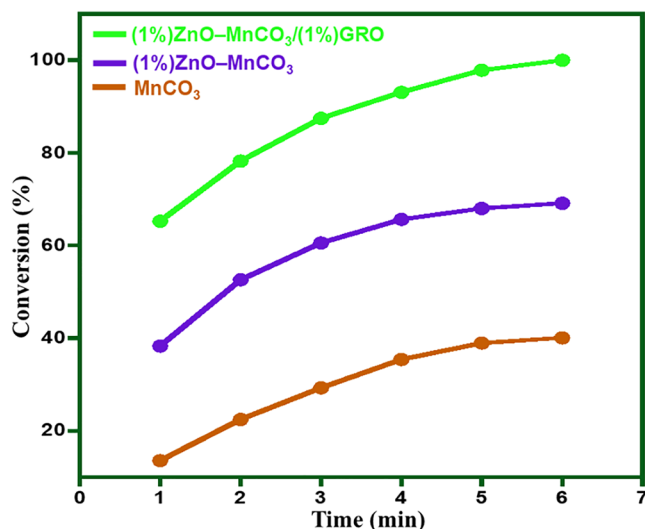


FIGURE 8 Effect of reaction time (min) on the catalytic performances of the as-synthesized catalysts

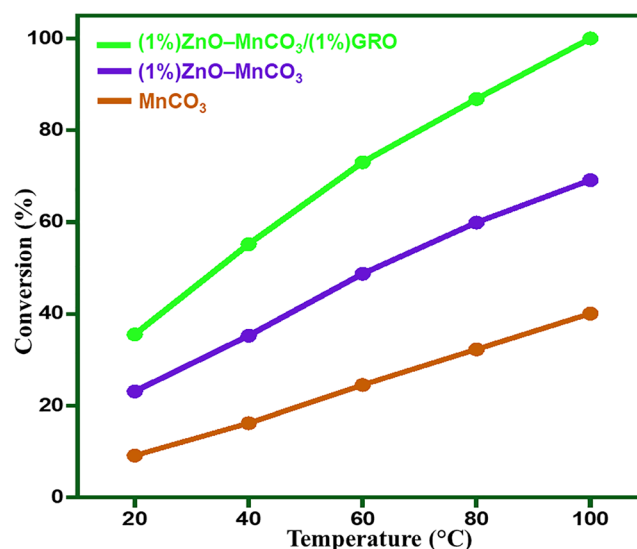


FIGURE 9 Impact of temperature on BzOH oxidation using the as-prepared catalysts

MnCO₃, yielded 69.1% conversion of BzOH after 6 min (1, entry 2). However, after modification of the catalytic protocol by doping it with 1 wt% of GRO, (1%)ZnO-MnCO₃/(1%)GRO exhibited highest catalytic performance of all the catalysts with different weight percentages of GRO. The (1%)ZnO-MnCO₃/(1%)GRO catalyst gave 100% conversion of BzOH in an extremely short time (6 min) and had a higher specific activity of 66.7 mmol.g⁻¹.hr⁻¹ (1, entry 3). On increasing the percentage of GRO to (1%)ZnO-MnCO₃/(3%)GRO, the catalytic efficiency slightly decreased and 92.3% yield of BzOH was obtained under similar conditions (1, entry 4). The nanocomposites with 5% and 7% GRO afforded 79.2 and 72.6% conversions, respectively, under the same catalytic conditions (1, entries 5 and 6). The reduction in the efficacy of the catalytic system was presumably due to the increase in the blocking effect of GRO, which can cover or block the active sites of the ZnO-MnCO₃ catalyst. The selectivity of BzH remained almost unchanged throughout the oxidation experiments (<99%) (1, entries 1–6). Consequently, it was deduced that the GRO plays a crucial role in improving the efficacy of the present catalytic system for this transformation.

3.2.2 | Impact of various graphene derivatives

We compared the catalytic efficacy of ZnO-MnCO₃ incorporated with various graphene derivatives (i.e., GRO and HRG) for aerial oxidation of BzOH to understand the function of graphene. The results are outlined in Table 2 and depicted in Figure 8. The undoped catalyst, that is,

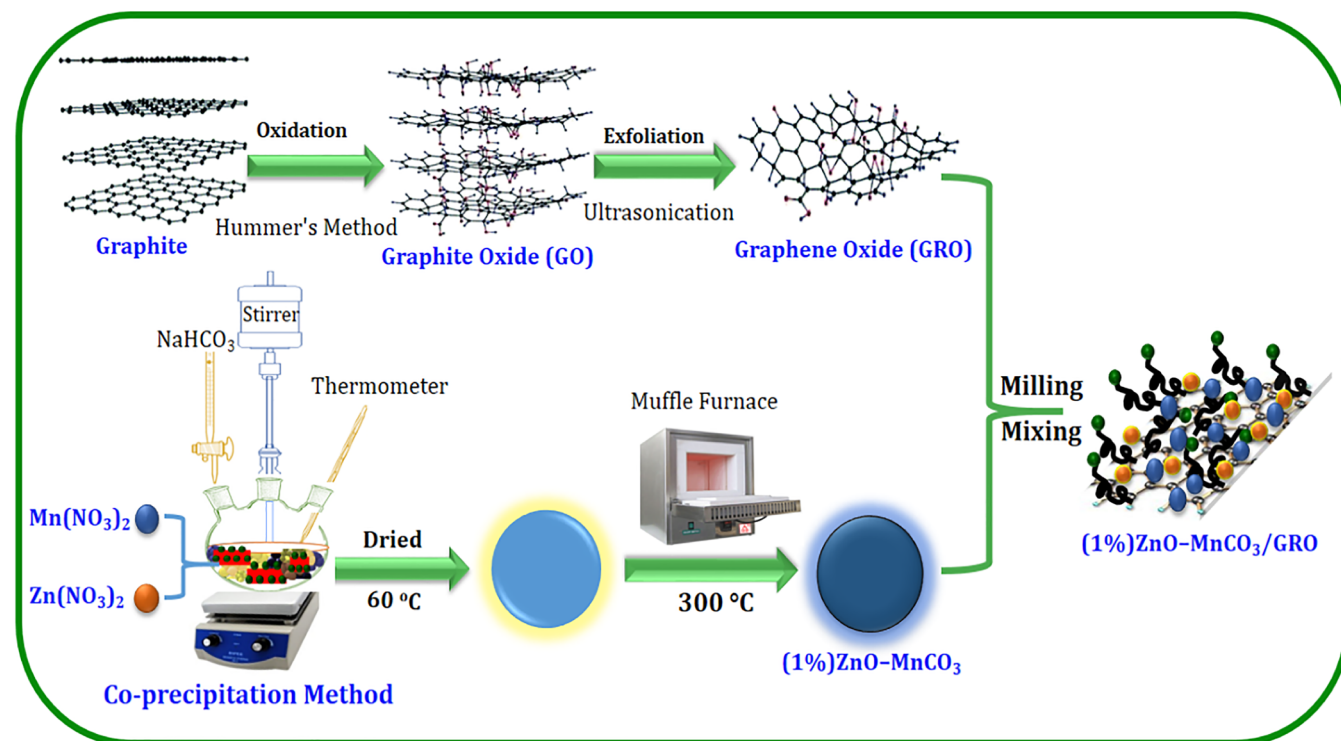


FIGURE 10 Impact of the amount of as-synthesized catalyst on the catalytic activity

MnCO_3 without ZnO NPs, afforded only 40% BzOH conversion within 6 min, but after doping it with 1 wt% of ZnO, that is, (1%)ZnO– MnCO_3 , the effectiveness markedly increased, and yielded 69% conversion of BzOH at the same conditions (entries 1 and 2). Using GRO as a catalyst dopant, that is, (1%)ZnO– MnCO_3 /(1%)GRO nanocomposite, yielded much higher catalytic efficiency than the catalyst doped with HRG, that is, (1%)ZnO– MnCO_3 /(1%)HRG nanocomposite. The (1%)ZnO– MnCO_3 /(1%)GRO catalyst exhibited complete transformation of BzOH within the very short period of 6 min with an outstanding specific activity of $67 \text{ mmol.g}^{-1}.\text{hr}^{-1}$ (entry 3). The excellent activity is probably due to the superabundant oxygen-carrying groups in GRO facilitating the oxidation of BzOH.⁴³ Importantly, after insertion of HRG in the catalytic protocol, the (1%)ZnO– MnCO_3 /

(1%)HRG nanocomposite gave higher catalytic performance compared with the undoped catalyst without HRG, the (1%)ZnO– MnCO_3 catalyst. The (1%)ZnO– MnCO_3 /(1%)HRG catalyst exhibited a 96.5% conversion of BzOH alongside a specific activity of $64.4 \text{ mmol.g}^{-1}.\text{hr}^{-1}$ (entry 4). The higher performance after using HRG in the catalytic system might be attributed to the increase of interaction between the π electrons on the aromatic alcohols and the π electrons on the surface of the HRG by strong π – π stacking near the catalytically active mixed metal oxides (i.e., ZnO– MnCO_3). It is also attributed to the prevention of aggregation of ZnO NPs due to the presence of HRG in the catalytic system in addition to the very high surface area that can homogeneously distribute the active sites of the catalysts, which leads to increase the surface area of the as-prepared nanocomposites,

TABLE 2 Catalytic BzOH oxidation over various synthesized catalysts

Entry	Catalyst	Surface area (m^2/g)	Conversion (%)	Specific activity ($\text{mmol.g}^{-1}.\text{hr}^{-1}$)	Selectivity (%)
1	MnCO_3	70.5	40.1	26.7	<99
2	(1%)ZnO– MnCO_3	120.3	69.1	46.1	<99
3	(1%)ZnO– MnCO_3 /(1%)GRO	244.6	100	66.7	<99
4	(1%)ZnO– MnCO_3 /(1%)HRG	239.1	96.5	64.4	<99

Note. Conditions: 2 mmol BzOH, 10 ml toluene, 300 mg catalyst, O_2 20 ml/min, 100°C , 6 min.

which in turn enhances the performance of the nanocomposites.

3.2.3 | Impact of temperature

Generally, the reaction temperature plays a fundamental role in the catalytic methodology and has an apparent impact on the effectiveness and selectivity of the catalyst. Thus, we conducted this reaction at different temperatures (RT, 40, 60, 80, and 100°C) in the presence of the catalysts (MnCO_3 , (1%)ZnO– MnCO_3 , and (1%)ZnO– MnCO_3 /(1%)GRO) while keeping the other reaction factors fixed. According to Figure 9, the reaction temperature has a positive impact on the activity of all the catalysts used in this study. Moreover, the selectivity of BzH achieved was <99% for all catalysts. The results indicate that the best catalyst, with the highest performance, is (1%)ZnO– MnCO_3 /(1%)GRO. At low temperatures (i.e., RT), a relatively smaller BzOH conversion of 35.5% was observed. Unsurprisingly, higher temperatures resulted in better catalyst performance. At 100°C, complete transformation of the alcohol was obtained under identical catalytic conditions. As a result, 100°C was chosen as the preferred temperature for this transformation.

3.2.4 | Impact of catalyst amount

To determine the influence of varying the quantity of catalyst (MnCO_3 , (1%)ZnO– MnCO_3 , (1%)ZnO– MnCO_3 /(1%)HRG, and (1%)ZnO– MnCO_3 /(1%)GRO), six different amounts (50, 100, 150, 200, 250, and 300 mg) were used while keeping all other parameters unchanged. The results are shown in Figure 10. It can be clearly seen that the conversion of BzOH increases linearly as the amount of catalyst is increased from 50 to 300 mg. Meanwhile, selectivity towards BzH is almost unchanged throughout all the oxidation experiments (<99%). Of all the catalysts used in this study (1%)ZnO– MnCO_3 /(1%)GRO exhibited the highest activity for this transformation. When the amount of catalyst was increased from 50 to 300 mg, the BzOH conversion linearly increased from 24.8% to 100% after just 6 min at 100°C. The study shows only 0.3 g of the catalyst was needed to obtain full oxidation of BzOH within an extremely short time. Thus, it can be stated that the activities of the as-obtained catalysts varied linearly with catalyst amount, as shown in Figure 10.

Under the optimum catalytic conditions, a blank process carried out in presence of (1%)ZnO– MnCO_3 /(1%)GRO catalyst using the solvent toluene without a substrate (BzOH) confirmed that the solvent does not perform any function in the BzOH oxidation. No formation

of BzH was observed by gas chromatography, implying that the desired BzH is produced from the catalytic oxidation of BzOH and not from toluene oxidation under these conditions. A blank reaction of the oxidation process performed in the absence of catalyst showed that the produced BzH is formed as a result of the catalytic performance of the as-made catalyst and not the auto-oxidation of BzOH. No formation of BzH was observed, confirming that our catalyst is indispensable for this transformation. Furthermore, to show the importance of the oxidizing agent (O_2), the reaction was conducted over (1%)ZnO– MnCO_3 /(1%)GRO catalyst using air without bubbling molecular O_2 . At optimum conditions the results showed a lower (32.6%) conversion of BzOH comparing with the 100% conversion achieved when the reaction was carried out while bubbling O_2 through it.

A probable mechanism can only be proposed by using *in situ* spectroscopic approaches. Nevertheless, according to the previously reported publications in the field of catalysis, the rate-determining step is typically the dehydrogenation step in any catalytic oxygenation of alcohols.^[44] However, we assume that this reaction obeys the Marvan–Krevelen oxidation mechanism, which was reported by Tang and his group^[45] and confirmed by others.

3.3 | Recovery studies

The recovery of heterogeneous catalysts for reuse and their stability are of massive importance in industrial applications. Therefore, the catalyst (1%)ZnO– MnCO_3 /(1%)GRO was subjected to recycling studies for aerial oxidation of BzOH with O_2 and the results are illustrated in Figure 11. The recycling results revealed that the prepared catalyst could be efficiently recycled five times without a significant decrease its efficiency after each cycle. BzOH conversion decreases slightly from 100% to 93.76% after five cycles, presumably due to the inevitable weight loss of catalyst during the centrifuge step.^[46] BzH selectivity was maintained at <99% during the recycling tests. These data confirm that the as-synthesized catalysts are resistant to deactivation in selective BzOH oxidation.

To further demonstrate the superior efficacy of the (1%)ZnO– MnCO_3 /(1%)GRO catalyst, this catalytic protocol was compared with that for previously reported Zn-containing catalysts, as shown in Table 3. The results show that the (1%)ZnO– MnCO_3 /(1%)GRO catalyst is the most effective of the listed Zn-based catalysts for BzOH oxidation in terms of conversion, reaction period, and specific activity. The (1%)ZnO– MnCO_3 /(1%)GRO catalyst achieved 100% conversion of BzOH and >99% selectivity towards BzH within a very short time (6 min) and had superior specific activity ($66.7 \text{ mmol.g}^{-1}.\text{hr}^{-1}$). According

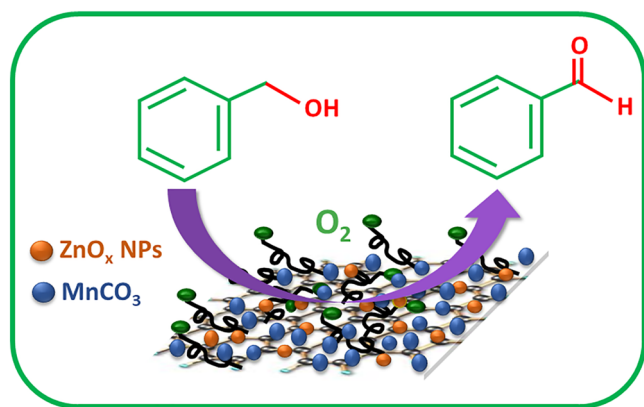


FIGURE 11 Reusability results for (1%)ZnO–MnCO₃/(1%)GRO in BzOH oxidation. Conditions: 2 mmol BzOH, 300 mg (1%) ZnO–MnCO₃/(1%)GRO catalyst, 20 ml/min O₂, 100°C, 6 min

to Table 3, the other Zn-based catalysts took longer to achieve complete transformation of BzOH and our catalyst has higher specific activity by comparing with other listed catalysts. For example, Liu et al.^[47] reported aerial selective oxidation of BzOH in the presence of Pt/ZnO catalyst using O₂ as a clean oxidizing agent in water as green solvent with BzOH conversion of 94.1%, 100% BzH selectivity, and calculated specific activity of about 0.2 mmol.g⁻¹.hr⁻¹ within 10 hr at RT. Albadi and his group^[48] also successfully synthesized a CuO–ZnO-supported gold NP catalyst (CuO–ZnO/Au NP) and used

it in the aerial oxidation of BzOH. The CuO–ZnO/Au NP catalyst exhibited 94% BzOH conversion and >99% BzH selectivity as well as specific activity of 18.8 mmol.g⁻¹.hr⁻¹ after 1 hr.

3.4 | General applicability of (1%)ZnO–MnCO₃/(1%)GRO catalyst

After optimization the catalytic conditions, these conditions were expanded to various kinds of alcohols (e.g., primary, secondary, aromatic, aliphatic, heterocyclic, and allylic) to show the versatility of the (1%)ZnO–MnCO₃/(1%)GRO catalyst. The results are collected in Table 4. It can be seen that all the primary aromatic alcohols were readily oxidized to their respective aldehydes with full conversion within short time periods (entries 1–22). Additionally, very high selectivities (above 99%) for the corresponding aldehydes and ketones were achieved for all the substrates in this study and no other products were produced in the reaction medium. It is evident that aromatic alcohols carrying electron-releasing substituents which possess sufficient electron density in the aromatic ring are oxidized more easily than alcohols with electron-withdrawing substituents.^[42,60] For example, *p*-methoxybenzyl alcohol, which contains an electron-releasing group, was completely transformed into *p*-methoxybenzaldehyde after 6 min (entry 3)

TABLE 3 Comparison between the effectiveness of the present catalyst and reported Zn containing catalysts

Catalyst	Conversion (%)	Selectivity (%)	T (°C)	Time	Specific activity (mmol.g ⁻¹ .hr ⁻¹)	Ref.
ZnO(1%)–MnCO ₃ /(1%)GRO	100	<99	100	6 min	66.7	Herein
ZnO(1%)–MnCO ₃ /(1%)HRG	100	<99	100	7 min	57.1	14c
Pt/ZnO	94.1	100	26	10 hr	0.2	47
CuO–ZnO/Au NP	94	<99	reflux	1 hr	18.8	48
Zn–Al LDH	100	100	reflux	2.5 hr	8.0	49
Ag NP/ZnO	98	<99	100	8 hr	24.5	50
ZnSA4	100	<99	80	8 hr	2.5	51
ZnBr ₂ /chloramine-T	96	<99	reflux	1.5 hr	6.4	52
ZnIn ₂ S ₄	100	<99	RT	2 hr	6.3	53
ZnPOM@APIB-MWCNT	95	<99	reflux	4 hr	2.4	54
ZnWO ₄	70	100	70	10 hr	0.7	55
PW ₁₁ Zn@AC	100	<99	reflux	0.75 hr	6.7	56
ZnPW ₁₂	80.1	89.1	90	3.5 hr	21.7	57
POM/Zn	100	100	reflux	4.5 hr	4.4	58
Zn NP/Fe ₂ O ₄	100	60	70	6.5 hr	7.7	59

Note. Zn–Al LDH–Zn–Al layered double hydroxides, ZnSA4–Strontium(II)-added zinc aluminate, ZnPOM@APIB-MWCNT–Zinc polyoxometalate immobilized on multi-wall carbon nanotubes modified with ionic liquid, PW₁₁Zn@AC–Zinc polyoxometalate immobilized on activated carbon, POM/Zn–Zinc polyoxometalates.

TABLE 4 Oxidation of various kinds of alcohols over (1%)ZnO–MnCO₃/(1%)GRO nanocomposite under base-free condition

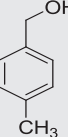
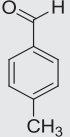
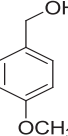
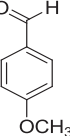
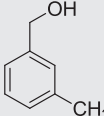
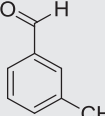
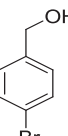
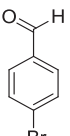
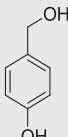
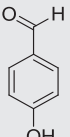
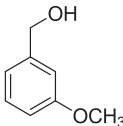
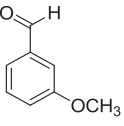
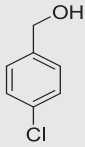
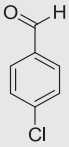
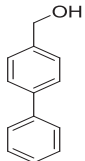
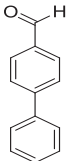
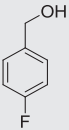
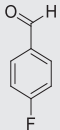
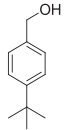
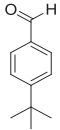
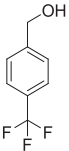
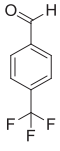
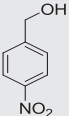
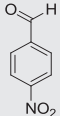
Entry	Alcohol	Product	Time (min)	Conversion (%)	Selectivity (%)
1			6	100	>99
2			6	100	>99
3			6	100	>99
4			7	100	>99
5			8	100	>99
6			8	100	>99
7			9	100	>99
8			10	100	>99

TABLE 4 (Continued)

Entry	Alcohol	Product	Time (min)	Conversion (%)	Selectivity (%)
9			11	100	>99
10			11	100	>99
11			12	100	>99
12			13	100	>99
13			14	100	>99
14			14	100	>99
15			16	100	>99

(Continues)

TABLE 4 (Continued)

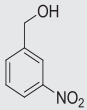
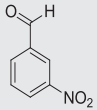
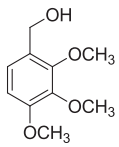
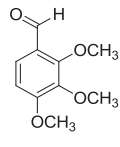
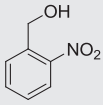
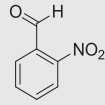
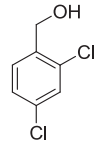
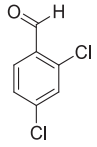
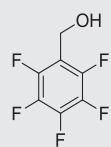
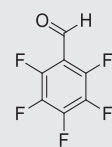
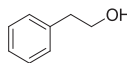
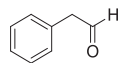
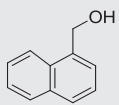
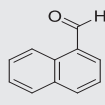
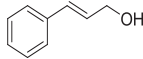
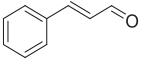
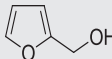
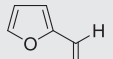
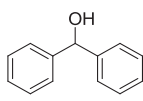
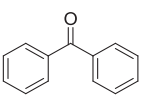
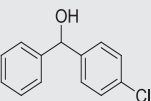
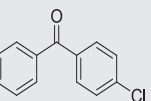
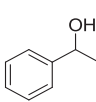
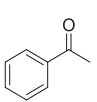
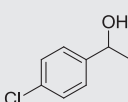
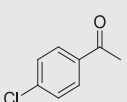
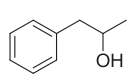
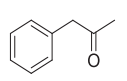
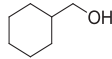
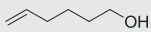
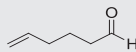
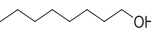
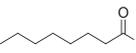
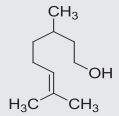
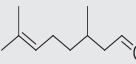
Entry	Alcohol	Product	Time (min)	Conversion (%)	Selectivity (%)
16			16	100	>99
17			18	100	>99
18			20	100	>99
19			20	100	>99
20			22	100	>99
21			15	100	>99
22			25	100	>99
23			10	100	>99

TABLE 4 (Continued)

Entry	Alcohol	Product	Time (min)	Conversion (%)	Selectivity (%)
24			25	100	>99
25			7	100	>99
26			12	100	>99
27			6	100	>99
28			10	100	>99
29			14	100	>99
30			20	100	>99
31			30	100	>99
32			100	100	>99

(Continues)

TABLE 4 (Continued)

Entry	Alcohol	Product	Time (min)	Conversion (%)	Selectivity (%)
33			110	100	>99
34			105	100	>99
35			35	100	>99
36			85	100	>99
37			110	100	>99

Note. Conditions: 2 mmol substrate, 300 mg (1%)ZnO–MnCO₃/(1%)GRO catalyst, 20 ml/min O₂, 100°C.

whereas *p*-(trifluoromethyl)benzyl alcohol, which has an electron-withdrawing group, required a relatively long reaction time of 14 min (entry 13). It can also be seen from Table 4 that substituents on the *para* position of aromatic alcohols are readily oxidized compared with substituents on the *ortho* and *meta* positions, maybe because the *para* derivatives have lower steric hindrance comparing with other positions.^[61] For example, *p*-methylbenzyl alcohol was completely oxidized to *p*-methylbenzaldehyde after just 6 min (entry 2), whilst *o*- and *m*-methylbenzyl alcohols were wholly transformed to their respective aldehydes after 7 and 13 min, respectively (entries 4 and 12). Steric resistance is also an important parameter that affects the oxidation rate since bulky substituents (e.g., trifluoromethyl, dichloro, trimethoxy, and pentafluoro) connected to aromatic ring reduce the rate of oxidation. This is probably due to the steric hindrance that impedes the oxidation of the alcohols carrying bulky groups (entries 13, 17, 19, and 20).^[62] With respect to allylic alcohols, cinnamyl alcohol was selectively

transformed to cinnamaldehyde within a short time (10 min; entry 23). Moreover, heterocyclic alcohols were efficiently oxidized, for example furfuryl alcohol was completely oxidized to furfural with <99% selectivity after 25 min (entry 24).

For typical secondary aromatic alcohols, complete conversion and selectivity towards corresponding ketones were accomplished (entries 25–30). Diphenylmethanol was selectively oxidized to benzophenone within a reaction time of 7 min, whereas 4-chlorodiphenylmethanol also exhibited 100% conversion but after a relatively longer period (12 min). This might be due to 4-chlorodiphenylmethanol having an electron-withdrawing substituent that deactivates the aromatic ring by reducing the electronic density (entries 25 and 26).

Unsurprisingly, the oxidation of aliphatic alcohols was more difficult than for their aromatic counterparts.^[63] The as-prepared catalyst was found to be efficacious for the oxidation of primary aliphatic alcohols to aliphatic aldehydes. For instance, full oxidation of

cyclohexyl methanol and 5-hexenol was achieved by prolonging the reaction period (entries 31 and 32). Compared to secondary benzylic alcohols, the oxidation of secondary aliphatic alcohols showed a lower performance towards this reaction (entries 35–37). Evidently, it was indispensable to prolong the reaction period, attributed to the oxidation of aliphatic secondary alcohols is much readily than the aromatic counterparts. As anticipated, full transformation of α -phenyl-ethanol took place within just 6 min, whereas the complete conversion of 2-octanol took 110 min (entries 27 and 37). In conclusion, the aerial method using (1%)ZnO–MnCO₃/(1%)GRO is influenced by both electronic and steric effects.

4 | CONCLUSIONS

Nanocomposites of ZnO NPs doped MnCO₃ co-doped with graphene oxide (GRO) were successfully synthesized and characterized. We also compared ZnO–MnCO₃, ZnO–MnCO₃/(1%)HRG, and ZnO–MnCO₃/(1%)GRO for the oxidation of BzOH using O₂ as a nature-friendly oxidant in the absence of any additives or alkalis. Under the optimum conditions, ZnO–MnCO₃/(1%)GRO nanocomposite exhibited better catalytic efficiency compared with ZnO–MnCO₃ and ZnO–MnCO₃/(1%)HRG catalysts for BzOH oxidation. This can be attributed to the incorporation of GRO, which has valuable properties such a huge surface area, superior chemical stability, high mechanical and thermal stability, and various oxygen-carrying groups, which are responsible for attaching the catalytically active metal NPs by electrostatic interactions and therefore homogeneously distributed the active sites of other catalyst components (i.e., ZnO–MnCO₃), which in turn increases the surface area and activity of the nanocomposites. The catalyst ZnO–MnCO₃/(1%)GRO achieves a 100% BzOH conversion and >99% BzH selectivity within very short time. Its superior specific activity (67 mmol.g⁻¹.hr⁻¹) is much better than that found in the previously reported literature. Compared with GRO, HRG has a higher reduced content and stronger π – π interactions, and therefore should show higher catalytic activity but this stronger interaction might result in the formation of more stable spectator species and hence show lower catalytic activity. The ZnO–MnCO₃/(1%)GRO catalyst efficiently catalyzed the oxidation of a variety of alcohols with O₂ under mild reaction conditions, which is in accordance with the requirements of green chemistry. Interestingly, aromatic alcohol oxidation is more readily attained than for aliphatic alcohols, maybe because of the strong π – π interactions in aromatic alcohols. The main advantages of this catalytic protocol are (a) facile work-up procedure; (b) low cost and clean oxidant; (c) no surfactants or bases are

required; (d) moderate catalytic conditions; (e) low-cost recoverable catalyst, (f) complete yield; (g) fast process; and (h) applicable to a broad range of alcohols. These features mean this catalytic protocol will be very useful in industry for the production of carbonyl compounds.

ACKNOWLEDGEMENTS

The authors extend their appreciation to the Deanship of Scientific Research at King Saud University for funding this work through the research group project No. RG-1436-032.

ORCID

Syed Farooq Adil  <https://orcid.org/0000-0002-2768-1235>

Mohammed Rafi Shaik  <https://orcid.org/0000-0003-2937-317X>

Muhsir Kuniyil  <https://orcid.org/0000-0001-8038-1381>

Mujeeb Khan  <https://orcid.org/0000-0002-4088-6913>

Aslam Khan  <https://orcid.org/0000-0002-7906-5653>

Mohammed Rafiq H. Siddiqui  <https://orcid.org/0000-0002-4703-0333>

REFERENCES

- [1] L. M. D. Martins, A. Ribeiro, S. Carabineiro, J. Figueiredo, A. Pombeiro, *Dalton Trans.* **2016**, 45, 6816.
- [2] S. Guadix-Montero, H. Alshammari, R. Dalebout, E. Nowicka, D. J. Morgan, G. Shaw, Q. He, M. Sankar, *Appl. Catal., A* **2017**, 546, 58.
- [3] F. P. Cossio, M. C. Lopez, C. Palomo, *Tetrahedron* **1987**, 43, 3963.
- [4] Y.-F. Liang, N. Jiao, *Acc. Chem. Res.* **2017**, 50, 1640.
- [5] a) R. Dun, X. Wang, M. Tan, Z. Huang, X. Huang, W. Ding, X. Lu, *ACS Catal.* **2013**, 3, 3063. b) Y. Hong, X. Yan, X. Liao, R. Li, S. Xu, L. Xiao, J. Fan, *Chem. Commun.* **2014**, 50, 9679.
- [6] M. Xie, X. Dai, S. Meng, X. Fu, S. Chen, *Chem. Eng. J.* **2014**, 245, 107.
- [7] a) M. Assal, M. Shaik, M. Kuniyil, M. Khan, A. Al-Warthan, M. Siddiqui, S. Adil, *Metals* **2018**, 8, 468. b) C. Ragupathi, J. J. Vijaya, S. Narayanan, S. Jesudoss, L. J. Kennedy, *Ceram. Int.* **2015**, 41, 2069.
- [8] A. Villa, D. Wang, D. S. Su, L. Prati, *Cat. Sci. Technol.* **2015**, 5, 55.
- [9] P. Pokharel, Q.-T. Truong, *Compos. Part B-Eng.* **2014**, 64, 187.
- [10] V. M. Shinde, E. Skupien, M. Makkee, *Cat. Sci. Technol.* **2015**, 5, 4144.
- [11] Z. Hu, Y. Zhao, J. Liu, J. Wang, B. Zhang, X. Xiang, *J. Colloid Interface Sci.* **2016**, 483, 26.
- [12] Y. Su, L.-C. Fan, Y.-M. Liu, Y. Cao, H.-Y. He, K.-N. Fan, *Cat. Com.* **2007**, 8, 2181.
- [13] J. Phiri, L.-S. Johansson, P. Gane, T. Maloney, *Compos. Part B-Eng.* **2018**, 147, 104.
- [14] a) J. Yan, Z. Fan, T. Wei, W. Qian, M. Zhang, F. Wei, *Carbon* **2010**, 48, 3825. b) T. Sreeprasad, S. M. Maliyekkal, K. Lisha, T. Pradeep, *J. Hazard. Mater.* **2011**, 186, 921. c) M. E. Assal, M. R. Shaik, M. Kuniyil, M. Khan, A. Y. Alzahrani, A. Al-Warthan, M. R. H. Siddiqui, S. F. Adil, *Catalysts* **2017**, 7, 391.

- [15] S. P. Lonkar, V. V. Pillai, S. Stephen, A. Abdala, V. Mittal, *Nano Micro Lett.* **2016**, *8*, 312.
- [16] A. Primo, M. Puche, O. D. Pavel, B. Cojocaru, A. Tirsoaga, V. Parvulescu, H. Garcia, *Chem. Commun.* **2016**, *52*, 1839.
- [17] F. Bonaccorso, A. Lombardo, T. Hasan, Z. Sun, L. Colombo, A. C. Ferrari, *Mater. Today* **2012**, *15*, 564.
- [18] W. Sun, X. Lu, Y. Tong, Z. Zhang, J. Lei, G. Nie, C. Wang, *Int. J. Hydrogen Energy* **2014**, *39*, 9080.
- [19] B. Zahed, H. Hosseini-Monfared, *Appl. Surf. Sci.* **2015**, *328*, 536.
- [20] Y. Liu, W. Jin, Y. Zhao, G. Zhang, W. Zhang, *Appl. Catal. Environ.* **2017**, *206*, 642.
- [21] Q. Zhao, C. Bai, W. Zhang, Y. Li, G. Zhang, F. Zhang, X. Fan, *Ind. Eng. Chem. Res.* **2014**, *53*, 4232.
- [22] C. Su, M. Acik, K. Takai, J. Lu, S.-j. Hao, Y. Zheng, P. Wu, Q. Bao, T. Enoki, Y. J. Chabal, *Nat. Commun.* **2012**, *3*, 1298.
- [23] J. Diao, H. Liu, J. Wang, Z. Feng, T. Chen, C. Miao, W. Yang, D. S. Su, *Chem. Commun.* **2015**, *51*, 3423.
- [24] C. Wang, L. Hu, Y. Hu, Y. Ren, X. Chen, B. Yue, H. He, *Cat. Com.* **2015**, *68*, 1.
- [25] a) E. Yoo, T. Okata, T. Akita, M. Kohyama, J. Nakamura, I. Honma, *Nano Lett.* **2009**, *9*, 2255. b) G. M. Scheuermann, L. Rumi, P. Steurer, W. Bannwarth, R. Mülhaupt, *J. Am. Chem. Soc.* **2009**, *131*, 8262. c) A. J. Shakir, D. C. Culita, J. Calderon-Moreno, A. Musuc, O. Carp, G. Ionita, P. Ionita, *Carbon* **2016**, *105*, 607.
- [26] W. S. Hummers Jr., R. E. Offeman, *J. Am. Chem. Soc.* **1958**, *80*, 1339.
- [27] P. K. Sandhya, J. Jose, M. S. Sreekala, M. Padmanabhan, N. Kalarikkal, S. Thomas, *Ceram. Int.* **2018**, *44*, 15092.
- [28] G. Xie, P. Xi, H. Liu, F. Chen, L. Huang, Y. Shi, F. Hou, Z. Zeng, C. Shao, J. Wang, *J. Mater. Chem.* **2012**, *22*, 1033.
- [29] S. Zhang, L. Zhu, H. Song, X. Chen, B. Wu, J. Zhou, F. Wang, *J. Mater. Chem.* **2012**, *22*, 22150.
- [30] S. F. Adil, M. E. Assal, M. Kuniyil, M. Khan, M. R. Shaik, A. Alwarthan, J. P. Labis, M. R. H. Siddiqui, *Mater. Express* **2017**, *7*, 79.
- [31] L. Geng, S. Wu, Y. Zou, M. Jia, W. Zhang, W. Yan, G. Liu, *J. Colloid Interface Sci.* **2014**, *421*, 71.
- [32] Y. Li, X. Lv, J. Lu, J. Li, *J. Phys. Chem. C* **2010**, *114*, 21770.
- [33] H. Hu, J.-y. Xu, H. Yang, J. Liang, S. Yang, H. Wu, *Mater. Res. Bull.* **2011**, *46*, 1908.
- [34] S. Yang, H. Yang, H. Ma, S. Guo, F. Cao, J. Gong, Y. Deng, *Chem. Commun.* **2011**, *47*, 2619.
- [35] T. Qiu, J. Wang, Y. Lu, W. Yang, *RSC Adv.* **2014**, *4*, 23027.
- [36] S. Gurunathan, J. W. Han, V. Eppakayala, J.-H. Kim, *Int. J. Nanomedicine* **2013**, *8*, 1015.
- [37] Y. Qi, H. Zhang, N. Du, D. Yang, *J. Mater. Chem.:A* **2013**, *1*, 2337.
- [38] P. Sharma, G. Darabdhara, T. M. Reddy, A. Borah, P. Bezboruah, P. Gogoi, N. Hussain, P. Sengupta, M. R. Das, *Cat. Com.* **2013**, *40*, 139.
- [39] H. P. Mungse, S. Verma, N. Kumar, B. Sain, O. P. Khatri, *J. Mater. Chem.* **2012**, *22*, 5427.
- [40] Ö. Metin, E. Kayhan, S. Özkar, J. J. Schneider, *Int. J. Hydrogen Energy* **2012**, *37*, 8161.
- [41] J. H. Kang, T. Kim, J. Choi, J. Park, Y. S. Kim, M. S. Chang, H. Jung, K. T. Park, S. J. Yang, C. R. Park, *Chem. Mater.* **2016**, *28*, 756.
- [42] C. Xu, L. Zhang, Y. An, X. Wang, G. Xu, Y. Chen, L. Dai, *Appl. Catal., A* **2018**, *558*, 26.
- [43] M. Miao, J. Feng, Q. Jin, Y. He, Y. Liu, Y. Du, N. Zhang, D. Li, *RSC Adv.* **2015**, *5*, 36066.
- [44] F. Z. Su, Y. M. Liu, L. C. Wang, Y. Cao, H. Y. He, K. N. Fan, *Angew. Chem. Int. Ed.* **2008**, *120*, 340.
- [45] Q. Tang, X. Gong, C. Wu, Y. Chen, A. Borgna, Y. Yang, *Cat. Com.* **2009**, *10*, 1122.
- [46] D. R. Dreyer, A. D. Todd, C. W. Bielawski, *Chem. Soc. Rev.* **2014**, *43*, 5288.
- [47] J. Liu, S. Zou, J. Wu, H. Kobayashi, H. Zhao, J. Fan, *Chin. J. Catal.* **2018**, *39*, 1081.
- [48] J. Albadi, A. Alihoseinzadeh, A. Razeghi, *Cat. Com.* **2014**, *49*, 1.
- [49] S. Hasannia, B. Yadollahi, *Polyhedron* **2015**, *99*, 260.
- [50] M. Hosseini-Sarvari, T. Ataee-Kachouei, F. Moeini, *Mater. Res. Bull.* **2015**, *72*, 98.
- [51] R. T. Kumar, N. C. S. Selvam, C. Ragupathi, L. J. Kennedy, J. J. Vijaya, *Powder Technol.* **2012**, *224*, 147.
- [52] P. Wang, J. Cai, J. Yang, C. Sun, L. Li, H. Hu, M. Ji, *Tetrahedron Lett.* **2013**, *54*, 533.
- [53] Z. Chen, J. Xu, Z. Ren, Y. He, G. Xiao, *J. Solid State Chem.* **2013**, *205*, 134.
- [54] R. Hajian, Z. Alghour, *Chin. Chem. Lett.* **2017**, *28*, 971.
- [55] S. R. Ede, A. Ramadoss, U. Nithiyanantham, S. Anantharaj, S. Kundu, *Inorg. Chem.* **2015**, *54*, 3851.
- [56] E. Assady, B. Yadollahi, M. Riahi Farsani, M. Moghadam, *Appl. Organomet. Chem.* **2015**, *29*, 561.
- [57] W. Tian, Y. Hou, X. Wang, B. Lu, J. Zhao, Q. Cai, *Chin. J. Chem.* **2012**, *30*, 433.
- [58] Z. Nadealian, V. Mirkhani, B. Yadollahi, M. Moghadam, S. Tangestaninejad, I. Mohammadpoor-Baltork, *J. Coord. Chem.* **2013**, *66*, 1264.
- [59] J. An, Y. Gou, C. Yang, F. Hu, C. Wang, *Mater. Sci. Eng. C* **2013**, *33*, 2827.
- [60] G. Wu, X. Wang, N. Guan, L. Li, *Appl. Catal. Environ.* **2013**, *136*, 177.
- [61] M. M. Kadam, K. B. Dhopte, N. Jha, V. G. Gaikar, P. R. Nemade, *New J. Chem.* **2016**, *40*, 1436.
- [62] R. Borthakur, M. Asthana, A. Kumar, R. A. Lal, *Inorg. Chem. Commun.* **2014**, *46*, 198.
- [63] G. Liu, J. Liu, W. Li, C. Liu, F. Wang, J. He, C. Guild, J. Jin, D. Kriz, R. Miao, *Appl. Catal., A* **2017**, *535*, 77.

SUPPORTING INFORMATION

Additional supporting information may be found online in the Supporting Information section at the end of this article.

How to cite this article: Adil SF, Assal ME, Shaik MR, et al. Efficient aerial oxidation of different types of alcohols using ZnO nanoparticle–MnCO₃–graphene oxide composites. *Appl Organomet Chem.* 2020;e5718. <https://doi.org/10.1002/aoc.5718>